

Real-time detection of Rydberg excitation dynamics of cold atoms in an optical cavity

Elmer Suarez and Sebastian Slama*

*Center for Quantum Science and Physikalisches Institut,
Eberhard-Karls Universität Tübingen, Auf der Morgenstelle 14, 72076 Tübingen, Germany*

(Dated: December 20, 2021)

We report on the real-time detection of internal-state dynamics of cold Rubidium atoms being excited from the ground state to the $30D_{5/2}$ Rydberg state via two-photon excitation in a ladder-type system. The atoms are first trapped and then released from a magneto-optic trap (MOT) positioned inside the mode of a low-finesse cavity. Then, Rydberg excitation is performed by a simultaneous pulse from two counter-propagating laser beams transverse to the cavity axis. This excitation changes the number of atoms able to absorb or emit cavity photons; thus, changing the collective atom-cavity coupling. We detect this by weakly driving the cavity and collecting the light transmitted through it with an avalanche photodiode (APD). We are able to observe not only the 2-photon excitation dynamics, but also the transfer of population out of the Rydberg state due to black-body radiation (BBR) and the decay back to the ground state.

I. INTRODUCTION

Rydberg atoms are hot candidates for realizing quantum gates [1, 2], quantum memories [3], single-photon devices [4, 5], and long-range interacting many-body quantum systems [6]. A key step for quantum experiments with Rydberg atoms is the coherent excitation of Rydberg states with high excitation probability [7, 8]. In this context, atomic ensembles in optical cavities are of particular interest due to the collective enhancement of light-matter interaction. Since the collective single photon Rabi frequency scales as $g_{\text{coll}} = g_0\sqrt{N}$ with coupling constant g_0 and atom number N , the required time for realizing a π -pulse decreases with $1/\sqrt{N}$ and thus makes it easier to overcome decoherence and loss.

Ensembles, however, suffer from shot-to-shot atom number fluctuations that limit the efficiency of the excitation. For that reason, excitation with high probability requires the precise knowledge of the atom number, or real-time monitoring of the excitation dynamics. In this regard, the cavity transmission can serve as a monitor for the number of atoms in the ground state. For a sufficiently high atom number resolution, this can even be used for spin squeezing [9, 10]. Recently, the cavity transmission has also been used to detect real-time atomic motion [11] and a dynamical phase transition in a cavity [12]. Here, the atom-cavity interaction is governed by stimulated absorption and emission of cavity photons. This makes the cavity blind to atoms with an energy, relative to the ground state, different to a cavity photon energy: a Rydberg state for this work. Therefore, detecting the cavity transmission is a real-time monitor for the Rydberg excitation dynamics. A complementary approach detecting the transmission through a superconducting microwave cavity to count Rydberg atoms has been recently demonstrated [13].

These approaches are based on the dispersive frequency shift due to the atoms, with the cavity far de-

tuned from the atomic resonance. They are in principle non-destructive, unlike detection by field ionization followed by ion-counting [14] or detection by fluorescence imaging [6]. Note that nondestructive detection of Rydberg atoms can also be achieved in free space using electromagnetically-induced transparency (EIT) [15]. Real-time detection of Rydberg excitations has also been observed in hot vapor cells by detecting the transmission of the laser driving the lower transition through a cell [16, 17].

We load Rb^{87} atoms into a MOT positioned within the mode of a cavity with finesse $F = 224$. Atoms are released and then excited from the $5S_{1/2}$ ground state to the $30D_{5/2}$ Rydberg state with $5P_{3/2}$ as intermediate state. This is accomplished by means of a simultaneous pulse from two counter-propagating beams transverse to the cavity axis, i.e. the pump beam driving the lower transition at 780 nm and the coupling beam driving the upper transition at 480 nm wavelength. At the same time, the cavity is driven by a weak probe field for detecting the collective atom-cavity coupling and, in turn, the number of atoms interacting with the cavity. The excitation pulse duration is 50 μs and, during this time, we initially observe the coherent excitation of atoms to the Rydberg state followed by the population of nearby Rydberg states induced by Black Body Radiation (BBR). After the pulse we observe the decay of all the populated states back to the ground state.

II. THEORETICAL BACKGROUND

The experimental scheme is sketched in Fig. 1a). It is convenient to separate the total system in two parts, each considering different types of atom-light interactions. In Sec. II A the atom-cavity interaction is introduced and simplifications are justified. Sec. II B introduces the atomic dynamics arising from the interaction with both transverse classical fields. At the end we show that it is possible to use the adiabatic approximation to unite both parts.

* sebastian.slama@uni-tuebingen.de

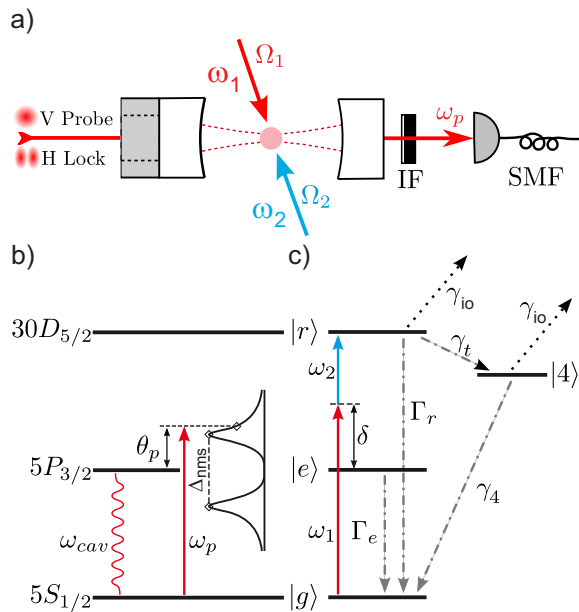


FIG. 1. a) Two transverse lasers with frequencies ω_1 and ω_2 excite atoms in the cavity to Rydberg states. A longitudinal laser with frequency ω_p probes simultaneously the atom-cavity system. The transmitted probe light transmitted through the cavity is filtered (IF=interference filter) from the lock light used to stabilize the cavity length, coupled into a single mode fiber (SMF), and detected by an avalanche photodiode. b) Relevant atomic levels of the atom-cavity interaction. The cavity resonance frequency is tuned in resonance with the lower transition generating a symmetric normal mode splitting $\Delta_{\text{nms}} = 2g_0\sqrt{N}$. The probe laser frequency is tuned to the slope of one of the normal modes. c) Atomic levels and decay rates involved in the Rydberg excitation.

A. Atom-cavity system

The description of our system starts considering a collection of two-level atoms interacting with a single mode cavity being driven by an external field. In this context, the single-atom cooperativity is introduced [18]:

$$C_1 = \frac{2g_0^2}{\kappa\Gamma_e}, \quad (1)$$

Where Γ_e and κ are the decay rates of the excited state and the cavity field, respectively. As will be explained in more detail in the next section, we have thousands of atoms interacting with the cavity and, at the same time, C_1 is on the order of 10^{-3} . Therefore, we apply the semi-classical approximation allowing us to neglect atom-photon correlations when writing the mean-field equations. This leads us to a widely used set of Maxwell-Bloch equations [18].

In order to calculate the intra-cavity photon number, we consider the driving field with frequency ω_p to be weak and introduce a probability $P = P_e + P_g$ for an atom to be in one of the two states $|g\rangle$ or $|e\rangle$, i.e. the states that are

coupled by the cavity field. The probability for the atom to be in any other state non interacting with the cavity field, in particular a Rydberg state, is correspondingly $1 - P$. Then, the steady-state for the normalized cavity photon number is given by

$$V = \left| \frac{1}{1 + i(\Delta - 2C_1N_{\text{eff}}P\chi)} \right|^2, \quad (2)$$

where $\Delta = 2(\theta_{\text{cav}} - \theta_p)/\kappa$, with θ_{cav} and θ_p the cavity and driving field detuning, relative to atomic resonance, N_{eff} the effective atom number inside the cavity mode volume, and $\chi = i/(1 - i2\theta_p/\Gamma_e)$ a factor proportional to the atomic susceptibility [18].

The classical field with Rabi frequency Ω_2 coupling the excited state to the Rydberg state (i.e. the coupling beam) is included into Eq. (2) by a modified susceptibility:

$$\chi' = \frac{i}{1 - i2\theta_p/\Gamma_e + \frac{\Omega_2^2/\gamma_R\Gamma_e}{1 - i2\vartheta_{\text{cav}}/\gamma_R}}. \quad (3)$$

Here, we have introduced the rate $\gamma_R = \Gamma_r + \gamma_d$ with the spontaneous decay rate Γ_r from the Rydberg state, and dephasing rate γ_d which will be introduced in the next section, and $\vartheta_{\text{cav}} = \theta_p + \theta_2$, with detuning θ_2 of the coupling beam relative to the upper atomic transition. Written in this way, it is easier to realize that the case $\vartheta_{\text{cav}} = 0$ generates a new resonance, i.e. electromagnetically induced transparency (EIT) through a cavity. Cavity Rydberg EIT has been studied in [19–21]. In our experiment, cavity Rydberg EIT (see Fig. 2) is used to benchmark the system in terms of Ω_2 and γ_R .

B. Two-photon Rydberg excitation

For a ladder-type system interacting with two classical fields (coupling and pump beam) the Hamiltonian can be written as

$$H = -\theta_1|e\rangle\langle e| - \vartheta_{\text{tr}}|r\rangle\langle r| + \frac{\Omega_1}{2}(\hat{\sigma}_{ge} + \hat{\sigma}_{eg}) + \frac{\Omega_2}{2}(\hat{\sigma}_{er} + \hat{\sigma}_{re}), \quad (4)$$

where $\hat{\sigma}_{ij} = |i\rangle\langle j|$, with $i, j = g, e, r$ (i.e. ground, excited and Rydberg); Ω_1 is the Rabi frequency for the pump beam, $\vartheta_{\text{tr}} = \theta_1 + \theta_2$ is usually called 2-photon detuning and θ_1 is the detuning of the pump beam relative to atomic resonance.

The transverse beams coherently drive the atoms from the ground state to the Rydberg state via the excited state. As shown in [22], the intermediate state can be adiabatically eliminated when θ_1 is sufficiently large, and an effective two-level Hamiltonian can be derived, with an effective Rabi frequency and an effective detuning :

$$\Omega_{\text{eff}} = \frac{\Omega_1\Omega_2}{\theta_1 - \theta_2}, \quad (5)$$

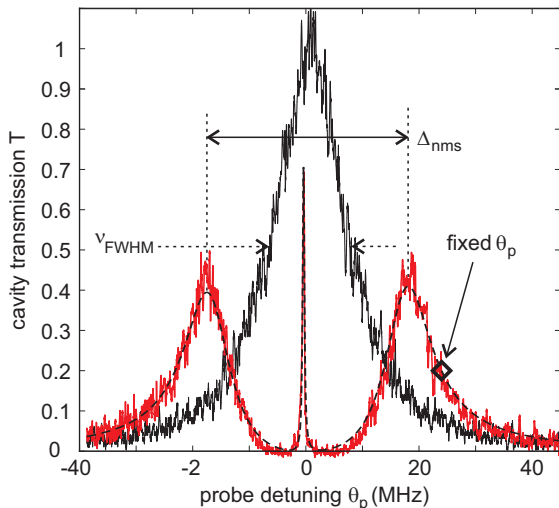


FIG. 2. Measured cavity transmission spectrum of the empty cavity (black) with full width at half maximum of $\nu_{\text{FWHM}} = 13.4$ MHz, and of the cavity filled with atoms and the coupling beam on (red), featuring a normal mode splitting Δ_{nms} corresponding to 7.500 atoms and a cavity Rydberg EIT signal. The Rabi frequency of the coupling laser $\Omega_2 = 2\pi \times 5.9$ MHz and the broadened linewidth $\gamma_R = 2\pi \times 100$ kHz of the Rydberg state are determined from the theoretical fit (black dashed line). The fixed probe light detuning $\theta_p = 2\pi \times 24$ MHz used for detecting the internal state dynamics is tagged. In each curve, the probe frequency has been scanned within 1.5 ms across the atomic resonance. The curves are normalized to the empty cavity transmission.

$$\vartheta_{\text{eff}} = \vartheta_{\text{tr}} + \frac{\Omega_1^2 - \Omega_2^2}{2(\theta_1 - \theta_2)}. \quad (6)$$

This allows us to estimate how fast and how much we populate the Rydberg state.

The decay is taken into account in terms of Lindblad operators:

$$L_e = \sqrt{\Gamma_e}|g\rangle\langle e|, \quad (7)$$

$$L_r = \sqrt{\Gamma_r}|e\rangle\langle r|, \quad (8)$$

$$L_d = \sqrt{\gamma_d}|r\rangle\langle r|, \quad (9)$$

where Γ_e and Γ_r are the spontaneous decay rates from the $|e\rangle$ ($5P_{3/2}$) and $|r\rangle$ ($30D_{5/2}$) state. Here, we have included the fact that the $|r\rangle$ state couples to the $|e\rangle$ state, not the $|g\rangle$ state. Stray electric and magnetic fields as well as frequency noise from the lasers contribute to the decoherence of the Rydberg state [21] and are taken into account in the dephasing rate γ_d .

In contrast to the excitation scheme based on the three levels $|g\rangle$, $|e\rangle$, and $|r\rangle$, the decay back to the ground state involves also other states. First of all, even though the main spontaneous decay channel for the Rydberg state is to the $5P_{3/2}$ state, it will spontaneously decay

to several others. Additionally, BBR at room temperature is responsible for transferring the population out to other, neighboring, states. Since neither of the transverse beams interact with these other states, they will only go back to the ground state via spontaneous decay. This also means that Γ_r in Eq. (7) cannot account for the decay rate of these other states. This problem has been approached in [23] and more simply in [24, 25]. The latter approach models BBR population transfer out of a Rydberg state by a decay rate γ_t to a fourth state which will, in turn, decay to the ground state with a rate Γ_4 , see Fig. 1c). An ionization rate γ_{io} from the Rydberg states is also included in order to account for atom losses from the system.

With the Hamiltonian in Eq. (4) and the Lindblad operators in Eq. (7, 8 and 9) we obtain a system of differential equations describing the time dynamics of the 3-level system. Here, we insert the decay and ionization rates γ_t , γ_4 , and γ_{io} introduced before phenomenologically. The results of these simulations are used to calculate the time dynamics of the cavity field given by Eq. (2) using the adiabatic approximation: the atom-cavity system reaches its steady-state on a timescale on the order of 200 ns, faster than the Rydberg dynamics. The latter takes place, for our experimental parameters, on a timescale given by Eq. (5) which is below 1 MHz. The Rydberg dynamics is then introduced into Eq. (2) by the probability P that an atom is either in $|g\rangle$ or $|e\rangle$. The results of these simulations are used to fit our data and thus derive the decay rates.

III. EXPERIMENT

A. Experimental setup

Fig. 1a) shows a schematic of the most relevant parts. The MOT is located inside the volume of a confocal cavity of 50 mm length. We consider the losses of our cavity to be accounted only by the transmission of the cavity mirrors resulting in a finesse of $F = 224$ and a full width at half maximum of $\nu_{\text{FWHM}} = 13.4$ MHz, see Fig. 2. The cavity is resonant with the $F = 2$ to $F' = 3$ transition of the D2 line from Rb⁸⁷. The single atom-cavity coupling equals $g_0 = 2\pi \times 185.1$ kHz after taking the average over the Zeeman sublevels. The cavity length is controlled by a piezo-transducer using the Pound-Drever-Hall (PDH) technique with one of the sidebands of an amplitude-modulated 786 nm ("lock") laser. The carrier frequency of the lock laser is stabilized to a stable high-finesse cavity and the sidebands are generated with an EOM driven with a GHz frequency generator.

Light from both lock and probe laser are coupled into the cavity using the same beam path, but with orthogonal polarizations. This allows us to discriminate the lock laser from the reflected light in order to generate the correct error signal. Furthermore, we use different transverse modes for both lasers: the probe resonates with the

fundamental TEM₀₀ mode while the lock laser resonates with the TEM₁₀ mode. Light transmitted through the cavity is filtered out by an optical bandpass filter and a single-mode fiber before detection by an APD. In this way, we manage to keep the lock light below the noise level of the APD while having enough power to generate an error signal. By changing the EOM's driving frequency we are able to control the cavity detuning relative to the atomic resonance.

Excitation to the $30D_{5/2}$ Rydberg state is done via two-photon absorption. In our experiment this is accomplished by two counter-propagating beams transverse to the cavity axis. For driving the lower transition we use light from the same laser as the probe beam but controlled by a different AOM, allowing the pump beam to have a frequency different from the probe. The transition from the intermediate to the Rydberg state is driven with light generated by frequency-doubling a 960 nm wavelength amplified external cavity diode laser (ECDL) using an LBO crystal inside a home-made bow-tie cavity. The frequency is controlled and set to a detuning of $\Delta_2 = -31.8$ MHz by Rydberg EIT spectroscopy in a Rb vapor cell [26]. An AOM controls the power (120 mW maximum) of this light. Both transverse laser beams are shaped with cylindrical lenses to fit the density profile of the atoms in the cavity mode.

B. Experimental procedure

The experiment starts with a thermal cold cloud of $N \sim 10^6$ Rb⁸⁷ atoms in a MOT where they are cooled in an optical molasses to a temperature of $T \sim 10$ μ K. Lasers are then switched off. After a short free fall of the cloud the initial time for our measurements is set, $t = 0$.

The overlap between the atom cloud and the cavity mode is optimized by maximizing the normal mode splitting Δ_{nms} , shown in Fig. 2. Using $\Delta_{\text{nms}} = 2g_0\sqrt{N}$, we derive the effective number of atoms $N \sim 7.500$ in the cavity. Similar to [19–21] we measure a cavity Rydberg EIT signal and analyze the data by fitting them with the steady-state equations from which we determine the Rabi frequency $\Omega_2 = 2\pi \times 5.9$ MHz driving the upper transition and the broadened linewidth $\gamma_R = 2\pi \times 100$ kHz of the Rydberg state, compared to the natural linewidth $\Gamma_r = 2\pi \times 38$ kHz [27]. Note, that these parameters during the measurements shown in Fig. 3 are even bigger with $\gamma_R = 2\pi \times 650$ kHz and $\Omega_2 = 2\pi \times 7.6$ MHz. This linewidth has been determined in separate measurements not shown here. We attribute this additional broadening to stray electric and magnetic fields.

For measuring the internal state dynamics of the atoms we fix the probe detuning at $\theta_p = +24$ MHz, tagged in Fig. 2. The detuning of the transverse pump beam is fixed at $\Delta_1 = +31.8$ MHz in order to fulfill the two-photon resonance condition with the coupling beam which has a detuning of $\Delta_2 = -31.8$ MHz. After 2 ms free fall of the atom cloud we turn on the probe laser.

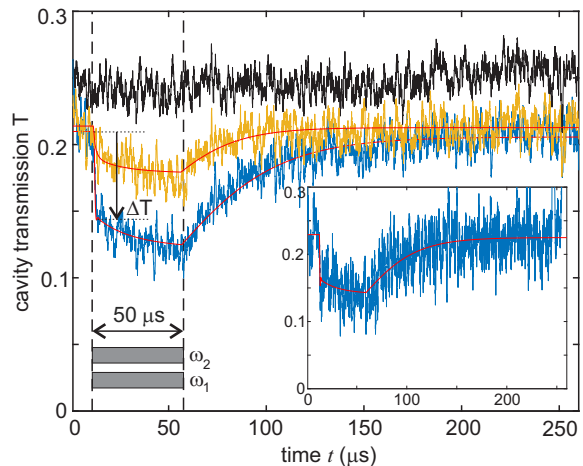


FIG. 3. Time signals of the cavity transmission. Atoms are excited to Rydberg states with $\Omega_2 = 2\pi \times 7.6$ MHz, $\Omega_1 = 2\pi \times 0.9$ MHz (orange) and $\Omega_1 = 2\pi \times 2.9$ MHz (blue). The black curve corresponds to $\Omega_1 = 2\pi \times 2.9$ MHz and $\Omega_2 = 0$ and is vertically shifted (+0.05) for clarity. The data in the main figure have been averaged over 10 repetitions of the experiment, the inset (same axes as the main figure) shows a single measurement, i.e. it is recorded in real-time. The red lines are fitted simulations of the master equation.

We wait for another 10 μ s in order for the cavity field to equilibrate, until we turn on both transverse beams simultaneously for a duration of 50 μ s.

Light transmitted through the cavity during the experiment has a power of ~ 2 nW which is just enough to be detected by an APD with 10 MHz bandwidth. This corresponds to ~ 200 photons inside the cavity per lifetime $\tau = 1/\kappa$ of the intracavity lightpower. The number of photons is thus very small compared to the number of ($N \sim 7.500$) atoms, such that the weak probe approximation is well justified.

IV. RESULTS

We analyze the transmission of the probe laser through the cavity. The signal is detected on a photodiode and electronically low-pass filtered with a timescale of 0.9 μ s. The resulting curve is shown in the inset of Fig. 3. Before the transverse beams are turned on at $t = 10$ μ s the signal corresponds to the steady-state value of the atom-cavity system driven at $\theta_p = +24$ MHz (see Fig. 2 for comparison). When the transverse beams are turned on, a fraction of the atoms are excited to the Rydberg level. This fraction no longer interacts with the cavity and thereby reduces the normal mode splitting. As a result, the transmission signal drops to a value corresponding to the new steady-state including Rydberg excitation. Coherent Rabi oscillations are not observed in this experiment due to decoherence. After the transverse beams are switched off at $t = 60$ μ s the atoms return to the ground state which makes the signal slowly return to its initial

value.

In order to analyze the excitation process and subsequent decay quantitatively with more precision, we average the recorded traces over 10 repetitions of the experiment. Fig. 3 shows averaged traces for different values of the Rabi frequency Ω_1 . An increasing Rabi frequency leads to more atoms excited to the Rydberg level and subsequently to a further reduced cavity transmission, i.e. a larger drop. In order to discern the internal state dynamics from motion of the atoms, which might be pushed out of the cavity mode due to photon recoil, we measure also the transmission, when the coupling laser is off, i.e. with $\Omega_2 = 0$. At the same time, the pump laser with its $\Delta_1 = +31.8$ MHz detuning to the D2 line pumps the atoms with a Rabi frequency of $\Omega_1 = 2\pi \times 2.9$ MHz. The resulting transmission (black curve in Fig. 3) is flat. This proves that light-scattering induced motion does not contribute to the observed signal.

We further want to analyze the steep drop at the beginning of the pulse. A fitted Rabi frequency $\Omega_1 = 2\pi \times 2.9$ MHz for the blue curve corresponds to an effective Rabi frequency given by Eq. (5) of $\Omega_{\text{eff}} = 2\pi \times 350$ kHz. The steady-state of this effective 2-level system should be reached on a timescale given by broadened linewidth $\gamma_R = 2\pi \times 650$ kHz: in our case $\sim 2 \mu\text{s}$, matching the observed timescale of the steep drop. Evidently from Fig. 3, the system has not yet reached steady-state after this timescale as the signal is continuously decreasing during the $50 \mu\text{s}$ pulse. This is caused by loss of atoms out of the 3-level system due to BBR-induced population redistribution to neighboring Rydberg states and due to spontaneous decay out of $30D_{5/2}$ to other states but the $5P_{3/2}$.

Using the Alkali Rydberg Calculator (ARC) [27], we identify the dominant decay channels from the $30D_{5/2}$ state back to the ground state. The spontaneous decay rate of the $30D_{5/2}$ is $\Gamma_r = 38.4$ kHz and is mainly (58%) back to the $5P_{3/2}$ state from where they quickly decay to the ground state. On the other hand, BBR population redistribution happens at a rate of $\gamma_t = 17.4$ kHz transferring to $F_{7/2}$, $P_{3/2}$ and $F_{5/2}$ states with probabilities of 58%, 39% and 3%, respectively. The most relevant decay channels are to the $28F_{7/2}$ and $29F_{7/2}$ states with rates 4.0 kHz and 2.8 kHz, respectively. They further decay with high probability (60%) to the $4D_{5/2}$ state with a rate of 35.5 kHz. From there, they will quickly decay via the $5P_{3/2}$ state to the ground state. Also, from the decays to $P_{3/2}$ states, 25% will decay to the $31P_{3/2}$ and $32P_{3/2}$ states with rates 1.6 kHz and 2.7 kHz, respectively. Next, they will decay (71%) to $D_{5/2}$ states with rates on the order of 2 kHz to the ones with $n = 4, 5, 6$. Taking the dominant decay channels into account with their relative weight, we estimate an effective decay rate back to the ground state $\gamma_4 = 27.4$ kHz.

When we turn off the transverse beams at $t = 60 \mu\text{s}$ we can see the decay of the atoms back to the ground state. Finally, we fit our data with the 4-level model explained above. The fitted curves are shown in red in Fig. 3.

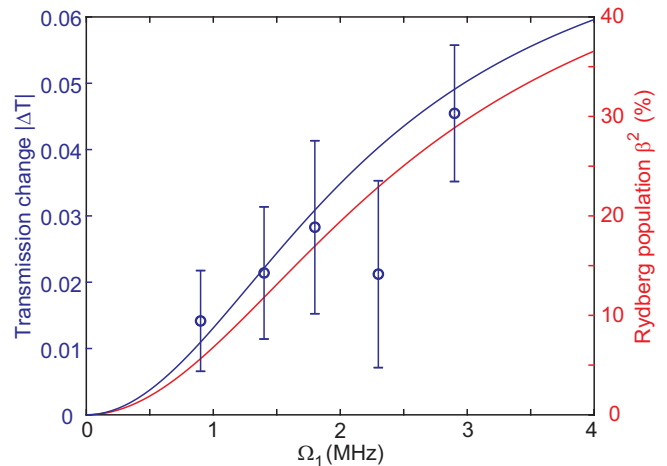


FIG. 4. Absolute change in cavity transmission $|\Delta T|$ (blue) induced by excitation of atoms into Rydberg states and the Rydberg population (red) as function of the pump's Rabi frequency Ω_1 . The coupling's Rabi frequency $\Omega_2 = 2\pi \times 7.6$ MHz is constant. The experimental data is determined from curves as shown in Fig. 3 and the error bars measured by the rms-noise of the signal. The blue and red curve have been determined by a simulation of the three level system.

The values obtained from the fits are $\gamma_t = 24.0$ kHz, $\gamma_4 = 34.6$ kHz and $\gamma_{io} = 500$ Hz. These values are comparable with the theoretical estimations derived above. We further analyze the steady-state cavity transmission and the corresponding occupation of the Rydberg state

$$\beta^2 = |\langle r|\Psi\rangle|^2 \quad (10)$$

of state $|\Psi\rangle$ as function of the Rabi frequency Ω_1 (before BBR takes place). For that purpose, we extract the cavity transmission directly after the steep drop from time tracks similar to those shown in Fig. 3. Thus, the effect of BBR-induced redistribution is negligible. We compare these data in Fig. 4 with the theoretical expectation based on simulations of the corresponding three-level system and its effect on the cavity transmission. In addition, we plot the occupation of the Rydberg state, given by the simulation. Fig. 4 shows that the experimentally data agree well with the simulation within their uncertainty. The simulation further shows that a considerable fraction of atoms up to 30% is excited to the Rydberg level.

V. CONCLUSIONS

We have shown that, taking advantage of the atom number dependence of the collective atom-cavity coupling, it is possible to observe Rydberg dynamics during excitation and decay. With ~ 7.500 atoms in a low finesse cavity, we observe Rydberg dynamics by monitoring the light transmitted through the cavity while weakly driving it at a fixed detuning of 24 MHz. Two laser

fields pump the atoms transversally to the cavity axis and excite them in a two-photon transition to a Rydberg state. At the beginning of the excitation the cavity transmission rapidly decays corresponding to the drive of the atoms to the Rydberg state. This is followed by a slow decay corresponding to population redistribution due to BBR-induced transitions and the various spontaneous decay channels involved. Finally, after turning off the pump lasers the transmission goes back to its initial value corresponding to the decay of atoms back to the ground state. These observations are corroborated by quantitative agreement with a 4-level model taking into account the excitation from the ground state to the Rydberg level via an intermediate state and an additional decay channel via a fourth level back to the ground state. The observations are real-time in the sense that each experimental run delivers a curve showing the complete dynamics. No sampling or averaging over several runs is required. Thus, the method can potentially be used for generating feedback to the system, for instance by controlling the length of the exciting pulse depending

on the current cavity transmission. This perspective is in particular interesting for cavities with higher finesse featuring single atom resolution and spin-squeezing. By improving the ratio between the effective Rabi frequency and the rate of decoherence it is possible to resolve Rabi oscillations in real-time. The presented method delivers also decay rates from the Rydberg state to neighboring states due to black-body radiation and their decay rates back to the ground state. A second perspective is thus to improve the precision of the method and use it for the precision measurements of BBR-induced decay.

ACKNOWLEDGMENTS

The project was funded by the Deutsche Forschungsgemeinschaft (DFG, German Research Foundation) - 422447846 and by ColOpt—EUH2020 ITN 721465. We acknowledge helpful discussions with Manuel Kaiser.

-
- [1] T. Wilk, A. Gaëtan, C. Evellin, J. Wolters, Y. Miroshnychenko, P. Grangier, and A. Browaeys, Entanglement of two individual neutral atoms using rydberg blockade, *Phys. Rev. Lett.* **104**, 010502 (2010).
- [2] L. Isenhower, E. Urban, X. L. Zhang, A. T. Gill, T. Henage, T. A. Johnson, T. G. Walker, and M. Saffman, Demonstration of a neutral atom controlled-not quantum gate, *Phys. Rev. Lett.* **104**, 010503 (2010).
- [3] L. Li and A. Kuzmich, Quantum memory with strong and controllable rydberg-level interactions, *Nat Commun* **7**, 13618 (2016).
- [4] H. Gorniaczyk, C. Tresp, J. Schmidt, H. Fedder, and S. Hofferberth, Single-photon transistor mediated by interstate rydberg interactions, *Phys. Rev. Lett.* **113**, 053601 (2014).
- [5] D. T. amd S. Baur, K. Schneider, S. Dürr, and G. Rempe, Single-photon transistor using a förster resonance, *Phys. Rev. Lett.* **113**, 053602 (2014).
- [6] P. Schauß, J. Zeiher, T. Fukuhara, S. Hild, M. Cheneau, T. Macri, T. Pohl, I. Bloch, and C. Gross, Crystallization in ising quantum magnets, *Science* **347**, 1455 (2015).
- [7] T. Cubel, B. K. Teo, V. S. Malinovsky, J. R. Guest, A. Reinhard, B. Knuffman, P. R. Berman, and G. Raithel, Coherent population transfer of ground-state atoms into rydberg states, *Phys. Rev. A* **72**, 023405 (2005).
- [8] J. Deiglmayr, M. Reetz-Lamour, T. Amthor, S. Westermann, A. de Oliveira, and M. Weidemüller, Coherent excitation of rydberg atoms in an ultracold gas, *Opt. Commun.* **264**, 293 (2006).
- [9] I. D. Leroux, M. H. Schleier-Smith, and V. Vuletic, Implementation of cavity squeezing of a collective atomic spin, *Phys. Rev. Lett.* **104**, 073602 (2010).
- [10] Z. Chen, J. G. Bohnet, S. R. Sankar, J. Dai, and J. K. Thompson, Conditional spin squeezing of a large ensemble via the vacuum rabi splitting, *Phys. Rev. Lett.* **106**, 133601 (2011).
- [11] R. D. Niederriter, C. Schlupf, and P. Hamilton, Cavity probe for real-time detection of atom dynamics in an optical lattice, *Phys. Rev. A* **102**, 051301(R) (2020).
- [12] T. W. Clark, A. Dombi, F. I. B. Williams, A. Kurko, J. Fortagh, D. Nagy, A. Vukics, and P. Domokos, Time-resolved observation of a dynamical phase transition of atoms in a cavity, arxiv:2106.03544 (2021).
- [13] S. Garcia, M. Stammeyer, J. Deiglmayr, F. Merkt, and A. Wallraff, Single-shot nondestructive detection of rydberg-atom ensembles by transmission measurement of a microwave cavity, *Phys. Rev. Lett.* **123**, 193201 (2019).
- [14] T. F. Gallagher, *Rydberg Atoms* (Cambridge University Press, 1994).
- [15] G. Günter, H. Schempp, M. R. de Saint-Vincent, V. Gavryusev, S. Helmrich, C. S. Hofmann, S. Whitlock, and M. Weidemüller, Observing the dynamics of dipole-mediated energy transport by interaction-enhanced imaging, *Science* **342**, 954 (2013).
- [16] B. Huber, T. Baluktsian, M. Schlagmüller, A. Kölle, H. Kübler, R. Löw, and T. Pfau, Ghz rabi flopping to rydberg states in hot atomic vapor cells, *Phys. Rev. Lett.* **107**, 243001 (2011).
- [17] T. Baluktsian, B. Huber, R. Löw, and T. Pfau, Evidence for strong van der waals type rydberg-rydberg interaction in a thermal vapor, *Phys. Rev. Lett.* **110**, 123001 (2013).
- [18] J. Gripp, S. L. Mielke, and L. A. Orozco, Evolution of the vacuum rabi peaks in a detuned atom-cavity system, *Phys. Rev. A* **56**, 3262 (1997).
- [19] R. Boddeda, I. Usmani, E. Bimbard, A. Grankin, A. Ourjountsev, E. Brion, and P. Grangier, Rydberg-induced optical nonlinearities from a cold atomic ensemble trapped inside a cavity, *J. Phys. B: At. Mol. Opt. Phys.* **49**, 084005 (2016).

- [20] J. Sheng, Y. Chao, S. Kumar, H. Fan, J. Sedlacek, and J. P. Shaffer, Intracavity rydberg-atom electromagnetically induced transparency using a high-finesse optical cavity, *Phys. Rev. A* **96**, 033813 (2017).
- [21] J. Ningyuan, A. Georgakopoulos, A. Ryou, N. Schine, A. Sommer, and J. Simon, Observation and characterization of cavity rydberg polaritons, *Phys. Rev. A* **93**, 041802 (2016).
- [22] E. Brion, L. H. Pedersen, and K. Mølmer, Adiabatic elimination in a lambda system, *J. Phys. A: Math. Theor.* **40**, 1033 (2007).
- [23] T. Zhou, B. G. Richards, and R. R. Jones, Absence of collective decay in a cold rydberg gas, *Phys. Rev. A* **93**, 033407 (2016).
- [24] K. J. Weatherill, J. D. Pritchard, R. P. Abel, M. G. Bason, A. K. Mohapatra, and C. S. Adams, Electromagnetically induced transparency of an interacting cold rydberg ensemble, *J. Phys. B: At. Mol. Opt. Phys.* **41**, 201002 (2008).
- [25] J. O. Day, E. Brekke, and T. G. Walker, Dynamics of low-density ultracold rydberg gases, *Phys. Rev. A* **77**, 052712 (2008).
- [26] R. P. Abel, A. K. Mohapatra, M. G. Bason, J. D. Pritchard, K. J. Weatherill, U. Raitzsch, and C. S. Adams, Laser frequency stabilization to excited state transitions using electromagnetically induced transparency in a cascade system, *Applied Physics Letters* **94**, 071107 (2009), <https://doi.org/10.1063/1.3086305>.
- [27] N. Šibalić, J. Pritchard, C. Adams, and K. Weatherill, Arc: An open-source library for calculating properties of alkali rydberg atoms, *Comput. Phys. Commun.* **220**, 319 (2017).